Title
Asphaltene Adsorption from Toluene onto Silica through Thin Water Layers

Journal
Langmuir, 35(2)

ISSN
0743-7463

Authors
Hu, Xiaozhen
Yutkin, Maxim P
Hassan, Saleh
et al.

Publication Date
2019-01-15

DOI
10.1021/acs.langmuir.8b03835

Peer reviewed

Asphaltene Adsorption from Toluene onto Silica through Thin Water Layers

Xiaozhen Hu,[†,§] Maxim P. Yutkin,[‡] Saleh Hassan,[‡] Jiangtao Wu,[§] J. M. Prausnitz,[†] and C. J. Radke*[,†,‡]

[†]Department of Chemical and Biomolecular Engineering, University of California Berkeley, Berkeley 94720, United States [‡] Ali I. Al-Naimi Petroleum Engineering Research Center (ANPERC), Physical Sciences and Engineering Division, King Abdullah University of Science and Technology (KAUST), Thuwal 23955-6900, Kingdom of Saudi Arabia [§] Key Laboratory of Thermo-Fluid Science and Engineering of Ministry of Education, Xi'an Jiaotong University, Xi'an 710049, China

*E-mail: radke@berkeley.edu

Abstract

Asphaltenes in crude oil play a pivotal role in reservoir oil production because they control rock-surface wettability. Upon crude oil invasion into a brine-filled reservoir trap, rock adherence of sticky asphaltene agglomerates formed at the crude oil/brine interface can change the initially water-wet porous medium into mixed-oil wetting. If thick, stable water films coat the rock surfaces, however, asphaltenic-oil adhesion is thought to be prevented. We investigate whether water films influence the uptake of asphaltenes in crude oil onto silica surfaces. Water films of known thickness are formed at a silica surface in a quartz crystal microbalance with dissipation and contacted by toluene-solubilized asphaltene. We confirm that thick water films prevent asphaltene molecular contact with the silica surface blocking asphaltene adhesion. The thicker the water film, the smaller is the amount of asphaltene deposited. Film thickness necessary for complete blockage onto silica is greater than about 500 nm, well beyond the range of molecular-chain contact. Water films of thickness less than 500 nm, sandwiched between toluene and solid silica, apparently rupture into thick water pockets and interposed molecularly thin water layers that permit asphaltene adherence.

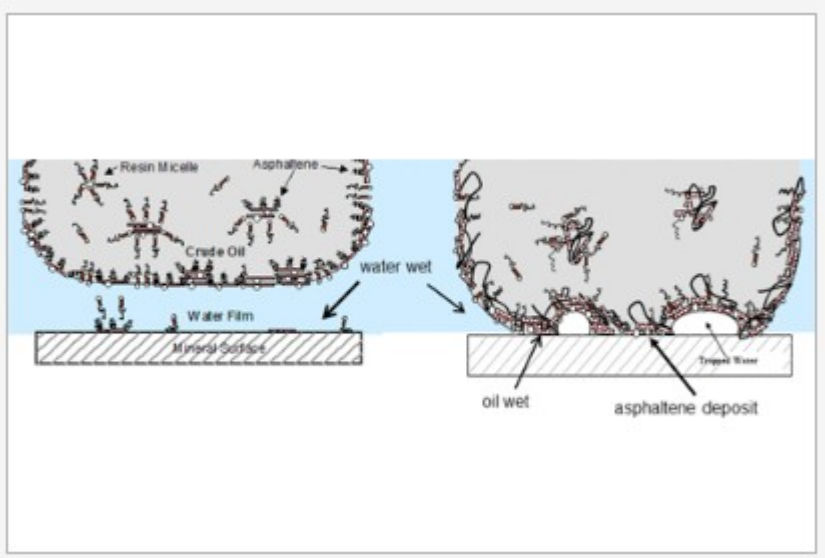

Introduction

Wettability of oil reservoir rock is crucial for devising efficient recovery processes.(1) Because oil reservoirs are produced by buoyant oil seeping into previously brine-filled traps, the reservoir rock is initially water-wet. As oil accumulates and water-volume fraction falls, however, many, perhaps all, oil reservoirs shift toward mixed-wet where portions of the rock surfaces are oil-wet and portions are water-wet, all within the same local pore space.(2,3) The key to this wettability alteration is the almost universal presence of asphaltenes in crude oil. Asphaltene molecules are defined as soluble in toluene but insoluble in alkanes. They are large sheet-like structures of interconnected heterocyclic rings that exhibit both polar and nonpolar moieties. Asphaltenes are water insoluble and readily aggregate in the oil phase.(4−7) Attachment of asphaltene aggregates to reservoir rock is widely believed to be the origin of mixed wetting.(2,8) However, because asphaltenes are not soluble in water, they cannot adsorb by reaching the rock surfaces through dissolution into the water phase. Kovscek et al.(2) propose that asphaltene aggregates adsorbed at the oil/brine interface directly deposit or stamp onto rock surfaces when intervening water films rupture during brine expulsion from a developing oil reservoir.

Figure 1 from Freer et al.(9) illustrates the proposed process of asphaltene deposition and wettability alteration. When oil invades a brine-filled rock, water-insoluble asphaltenes in the crude oil congregate irreversibly at the oil/brine interface.(7,9−11) Rock surfaces are initially protected by thick intervening water layers (Figure 1a). Water-soluble maltenes and resins may leach into the brine phase and adsorb on rock minerals. This adsorption process, however, is apparently not cohesive enough to shift rock wettability significantly. As oil continues to invade, water further drains, leaving thin water layers between the rock and oil/brine interfaces. When thin enough, the water films may rupture directly depositing (i.e., stamping) sticky asphaltene moieties onto the rock minerals (Figure 1b). Where water films

break, oily asphaltene aggregates coat the rock transforming it to locally oil-wet, primarily at the asperities of exposed surface roughness.(12,13) In rock crevices and corners covered by thick water pockets, however, the rock remains water-wet. This scenario produces “mixed-wet” oil reservoirs.(2,3)

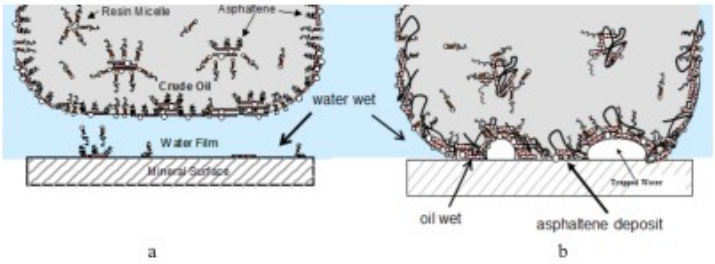

Figure 1. Stamping of asphaltene agglomerates (skins) formed at the crude-oil/brine interface. (a) Before film rupture. Adsorption of water-soluble polar solutes do not significantly alter wettability. (b) Onto mineral surfaces upon rupture of protective water films. Rupture process leaves patches of brine on the surface. After Freer et al.[9] with permission.

The primary supposition underlying mixed-wet oil reservoirs is that water films protect against asphaltene contact with the rock surfaces and, thus, do not allow oil adhesion.(14,15) To test this supposition, we investigate whether thin water films on a water-wet mineral surface prevent oil-solubilized asphaltenes from depositing. Gonzales and Taylor(16) tackled this problem by exposing quartz powder to air of varying water vapor relative humidity and then measuring the amount of asphaltene uptake from toluene by concentration depletion. Water film thickness on quartz surfaces for each relative humidity was obtained independently by Asay and Kim(17) using attenuated total reflection–infrared spectroscopy. We also consider asphaltene dissolved in toluene adsorbing through water films onto silica. However, we focus on water films deposited by withdrawing bulk liquid water from a water-wet silica surface placed in a quartz crystal microbalance with dissipation (QCMD) flow cell, akin to how water drains from pores during maturation of an oil reservoir. Excellent reviews are available on the application of QCMD to adsorption phenomena.(18,19)

Experiments and Methods

Chemicals

Toluene (99.9%, Fisher Chemicals) was used as received to dissolve asphaltene B6 powder kindly provided by Kilpatrick.(20) Detailed properties of the B6 asphaltene sample are available in Tables 2–5 of Spieker et al. (20) A stock solution of 1 g/L was prepared and stored in a fume hood. Lower concentrations of asphaltene were diluted from the stock solution by adding the desired amount of toluene. Distilled/deionized water was from a Milli-Q water system (Synergy, EMD Millipore Corporation), giving resistivity greater than 18.2 MΩ·cm at 25 °C.

Apparatus and Procedures

The QCMD instrument was from Biolin Scientific (Model E4, Gothenburg, Sweden). Manufacture-supplied silica-coated quartz sensors (AT-cut, 5 MHz,

QXS 303) were used as the adsorbent. Initially, and after each use, silica sensors were cleaned by the following procedure. Sensors were first rinsed with Milli-Q water followed by blow-drying with nitrogen. The sensors were then placed in an air plasma cleaner (Harrick Plasma Cleaner, 110 V, PDC-32G, medium intensity) for 10 min. Atomic force microscopy (Bruker Dimension Icon Model, Bruker Corporation, Massachusetts, CA, USA) was used to evaluate the resulting root mean square surface roughness of selective initially cleaned silica sensors at approximately 1 nm under air tapping mode in agreement with the literature.(21) After cleaning, the sensors were immediately transferred into the flow module (QFM 401) of the QCMD instrument and aligned to the desired position. To ensure repeatability, each sensor was normally used for no more than five times. An exception was for those experiments with asphaltene irreversibly adsorbed onto dry silica where pristine sensors were used. Temperature was set constant at 25 °C. Temperature equilibration for 30–60 min was allowed before initiating flow experiments.

For asphaltene adsorption studies onto dry silica, pure toluene was first injected into the QCMD flow cell by a peristaltic pump (ISMATEC, ISM935C) installed with 2-Stop Viton tubing (0.64 mm i.d., Cole-Parmer) at 100 μL/min. Resonant frequency and dissipation kinetics of the first, third, fifth, seventh, and ninth overtones were recorded simultaneously. Flushing was continuous for about 1–2 h until a stable baseline was achieved, defined by a frequency shift of each overtone of less than 0.2 Hz per hour. Asphaltene adsorption was then measured by injecting a sequence of increasing concentrations of asphaltene dissolved in toluene from 1 to 1000 mg/L. After each concentration increase, toluene flushing was performed to test for possible desorption.

For asphaltene uptake measurement out of toluene through an intervening water layer, a stable air baseline was first achieved. Milli-Q water was then pumped for 30–40 min. Next, water films were formed above the sensor surface by connecting the flow-cell outlet to a laboratory vacuum supply, allowing slow removal of bulk liquid water and replacement with ambient air. Depending on vacuum duration, water layers of various thicknesses were obtained. Details of water-film formation are described below. Pure toluene was injected following water-layer deposition. Next, an asphaltene-in-toluene solution (15 mg/L, water-saturated toluene) flowed into the QCMD cell. Finally, at the end of each flow experiment, excess toluene was flushed through the entire system. The cell was disassembled, and the sensor was cleaned as described above.

QCMD Theory

To interpret the observed QCMD frequency and dissipation signals, we adopt the continuum mechanics framework of Voinova et al.(22)Figure 2 displays the case of a homogeneous thin water film of thickness h_L covered by a second semi-infinite immiscible fluid, for example, oil or air. Both the water

layer and the covering fluid are Newtonian and incompressible and contain no adsorbing species. Continuum momentum balances are written for the thin liquid layer and for the immiscible overlayer fluid and coupled through no-slip and stress-continuity boundary conditions. Once expressions for the velocity profiles are established, the friction force by the thin liquid layer on the oscillating crystal, F_f, divided by the velocity amplitude of the crystal, V_o, is calculated to evaluate a beta factor: $\beta \equiv F_f/V_o$.(22) We find that

$$\beta = \eta_L k_L (1 + \Gamma)\frac{1 - A\, e^{2ik_L(h_L - h)}}{1 + A\, e^{2ik_L(h_L - h)}} \quad (1)$$

Where

$$A = \frac{1 + \eta k/\eta_L k_L}{1 - \eta k/\eta_L k_L} \quad (2)$$

ρ_L and η_L are density and viscosity of the water layer, respectively, and ρ and η are density and viscosity of the bulk overlayer fluid, respectively. k_L and k in eq 2 are wave numbers or inverse characteristic decay lengths of the thin water layer and the bulk covering fluid defined, respectively, by $k_L = \sqrt{\rho_L \omega/2\eta_L}$ and $k = \sqrt{\rho\omega/2\eta}$. $\omega = 2\pi n f^*$ is the angular frequency where f^* is the fundamental resonant crystal frequency in air or vacuum (4.95 MHz) and n is the overtone number (1, 3, 5, etc.). Equation 2 differs algebraically from that of Voinova et al.(22) (compare eq 11 of that manuscript). In the case of air as the covering immiscible fluid, $A = 1$.

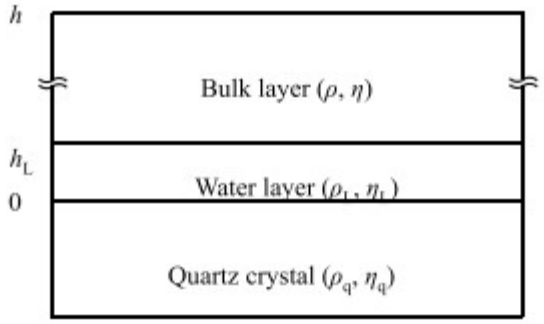

Figure 2. Schematic of the QCMD crystal covered by a thin water layer of thickness h_L, immersed in a covering fluid of semi-infinite thickness. Densities and viscosities of each compartment are labeled by ρ and η, respectively.

Given the beta factor, predicted frequency and dissipation shifts in QCMD follow from eq 15 of Voinova et al.(22) In the two-fluid case of eqs 1 and 2, we find that

$$\frac{\Delta\Gamma_n}{n} = \frac{\eta_L k_L}{2\pi\rho_q h_q}\frac{1 - A^2 e^{2ik_L h_L} - 2A\, e^{2ik_L h_L}\sin 2h_L k_L}{1 + A^2 e^{2ik_L h_L} + 2A\, e^{2ik_L h_L}\cos 2h_L k_L} \quad (3)$$

And

$$\Delta D_n = -\frac{\eta_L k_L}{n\pi f^* \rho_q h_q} \frac{1 - A^2 e^{-2h_L k_L} + 2A e^{-h_L k_L} \sin 2h_L k_L}{1 + A^2 e^{-2h_L k_L} + 2A e^{-h_L k_L} \cos 2h_L k_L} \quad (4)$$

where h_q is the thickness of the quartz crystal (0.334 mm) and ρ_q is its mass density (2648 kg/m^3).

Equations 3 and 4 are not restricted to thin water layers. Beyond a thickness of $3/k_L \approx 750$ nm, the water-layer thickness is effectively infinite. Equations 3 and 4 simplify to

$$\frac{\Delta f_n}{n} = -\frac{\eta_L k_L}{2\pi\rho_q h_q} = -\frac{1}{n^{1/2}} \frac{\sqrt{f^* \rho_L \eta_L}}{2\rho_q h_q} \quad (5)$$

And

$$\Delta D_n = \frac{\eta_L k_L}{n\pi f^* \rho_q h_q} = \frac{1}{n^{1/2}} \frac{1}{\rho_q h_q \sqrt{\pi f^*}} \sqrt{\rho_L \eta_L} \quad (6)$$

Frequency shifts are negative, whereas dissipation shifts are positive. Properties of the covering fluid no longer contribute at large water-film thickness. Equations 5 and 6 thus apply to any fluid-filled cell (with no solute adsorption).

For thin water films where $h_L k_L \ll 1$, eqs 3 and 4 reduce to

$$\frac{\Delta f_n}{n} = -\frac{f^* \rho_L h_L}{\rho_q h_q} \left| 1 - \frac{\rho\eta}{\rho_L \eta_L} \right| - \frac{1}{n^{1/2}} \frac{\sqrt{f^* \rho_L \eta_L}}{2\rho_q h_q} + O(h_L k_L)^2 \quad (7)$$

And

$$\Delta D_n = \frac{1}{n^{1/2}} \frac{1}{\rho_q h_q \sqrt{\pi f^*}} \sqrt{\rho\eta} + O(h_L k_L)^2 \quad (8)$$

To order thickness squared, only the fluid properties of the covering layer contribute to dissipation. The frequency shift for thin water layers, however, is influenced both by the mass of the water layer (i.e., $\rho_L h_L$) and by the overlayer fluid properties.

Figure 3 shows frequency shift from eq 3 as a function of water-layer thickness when the covering overlayer is air (i.e., $\rho\eta = 0$) for two overtone numbers 1 and 5. We rely on the fifth overtone experimentally because it is typically more precise. For large water-layer thicknesses, the frequency shift approaches that of a bulk water layer in eq 5. Water layers beyond a thickness of 500 nm are equivalent to a QCMD cell filled with water. At small film thicknesses, a linear decline regime appears in agreement with eq 7. Similar results for dissipation are obtained from eq 4 and highlighted in Figure 4. In accordance with eq 8, an asymptotic approach to zero thickness is now quadratic, rather than linear in Figure 3.

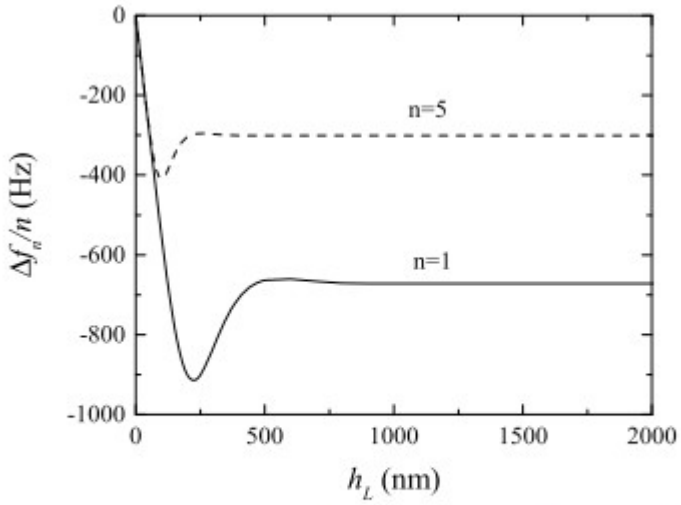

Figure 3. Predicted frequency change for a water film covered by air as a function of layer thickness h_L. First and fifth frequency overtones are calculated from eq 3.

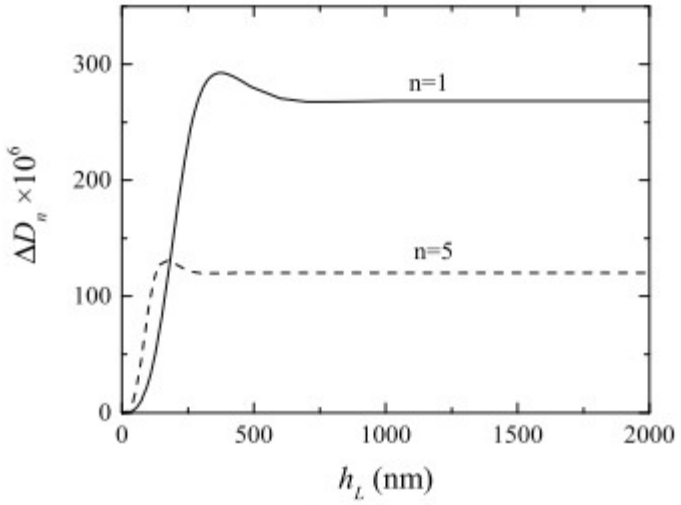

Figure 4. Predicted dissipation change for a water film covered by air as a function of layer thickness h_L. First and fifth frequency overtones are calculated from eq 4.

We study the role of a thin water layer on the adsorption of asphaltene from crude oil solubilized in a toluene overlayer. As justified later, the adsorbed asphaltene layer is approximated as homogeneous and rigid. For dilute asphaltene concentrations that do not influence toluene viscosity and density, continuum theory is a simple extension of eq 3

$$\frac{\Delta f_n}{n} = \frac{f^{1/2}\rho_l \eta_l k_l}{2\pi\mu_q k_q} \frac{1 - A^2 e^{2k_l h_L} + 2A e^{2k_l h_L} \sin 2k_l h_L}{1 + A^2 e^{2k_l h_L} + 2A e^{2k_l h_L} \cos 2k_l h_L} \quad (9)$$

or of eq 7 for a thin water film

 (10)

where Γ̃ is the toluene-dissolved asphaltene-solute mass uptake per unit area. The inverse of the ratio of instrument parameters multiplying solute adsorption in eqs 9 or 10 equals 17.7 ng/(cm^2 Hz) for a 5-MHz AT-cut quartz crystal and is commonly given the symbol C. The first term on the right of eq 9 or 10 is the classical result of Sauerbrey.(23) Dissipation in eq 4 or 8 for a thin intervening water layer is unchanged upon asphaltene adsorption because a rigid (or purely elastic) adsorbed layer suffers no viscous loss.

Equations 3–10 are relative to a baseline of the crystal oscillating in air (or vacuum). With other baseline choices, theory for that baseline is subtracted from the theory appropriate for the measured frequency and dissipation kinetics.

Deposition of Thin Water Films

To deposit a thin water film of known thickness between the silica surface and the toluene oil phase, we rely on the water-wetting properties of the QCMD flow cell. Water tends to reside adjacent to the silica surface in the flow cell, completely displacing nonwetting toluene. Conversely, toluene does not completely displace water in a cell but leaves a water film adjacent to the silica surface.(24,25)Figure 5 confirms this behavior. Initially, in Figure 5, toluene is flushed through the cell giving a zero baseline signal. Pure water is then injected, causing frequency to fall and dissipation to rise sharply. Dashed lines show the theoretical predictions from eqs 5 and 6 for a water-filled cell relative to a toluene-filled cell baseline. Excellent agreement is found using known viscosities and densities of water and toluene. Thus, water completely displaces immiscible toluene from the flow cell containing a silica floor. After about 40 min of water injection, toluene is again flushed. No change occurs in either frequency or dissipation. The explanation is that a thick water layer beyond 500 nm remains adjacent to the silica surface that appears infinite to the oscillating crystal. This observation allows us to deposit water films on the silica surface of varying thickness and then inject toluene without displacing the intervening water layer.

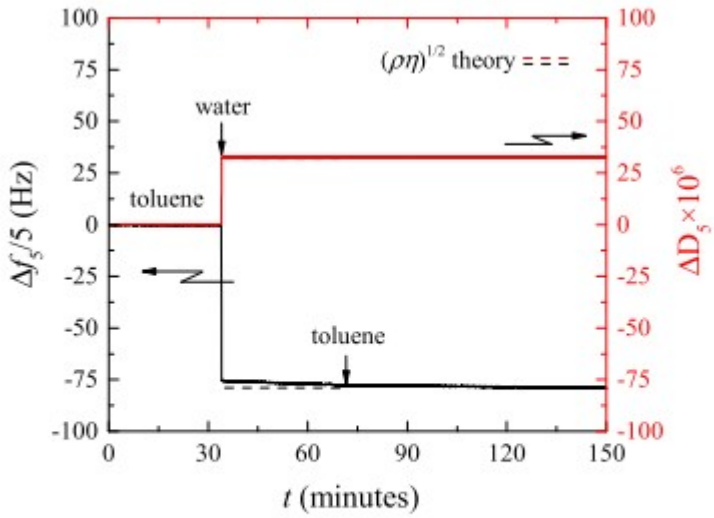

Figure 5. Frequency (black) and dissipation (red) kinetics (fifth overtone) relative to the toluene baseline for the injection sequence toluene, water, and toluene.

To establish the initial water-film thickness, we open the flow inlet to air and apply a slight vacuum to the flow outlet of an initially water-filled QCMD cell. During this process, we observe frequency and dissipation kinetics. By stopping water withdrawal at various times, finite-thickness water films remain on the silica surface.

Figure 6 illustrates the film deposition process. At 12 min, water fills the empty cell. Frequency declines and dissipation increases obeying theory in eqs 5 and 6, as shown by dashed lines. Water withdrawal in curve 2 starts at 80 min and lasts until about 100 min when withdrawal stops. At that time, frequency and dissipation stabilize. Theory in eq 3 (with $A = 1$) specifies a water-layer thickness near 16 nm. Similar results hold for curves 1 and 3 with curve 1 representing essentially dry silica ($h_L \approx 0$) and curve 3 representing a thick water film ($h_L > 500$ nm). Different water-film thicknesses are achieved by choosing different withdrawal-stoppage times.

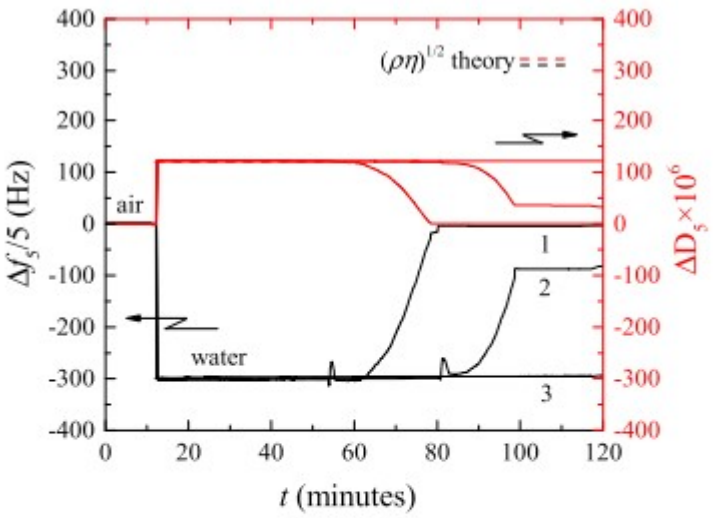

Figure 6. Frequency (black) and dissipation (red) kinetics (fifth overtone) relative to the air baseline for three water-withdrawal stoppages after (1) 30 min; (2) 20 min; and (3) no withdrawal stoppage. Curve 1 corresponds to essentially dry silica (without water layer). Curve 2 exhibits a thin water layer ~16 nm, and curve 3 corresponds to silica covered by thick, bulk water. Spikes correspond to initiation of water withdrawal.

Results and Discussion

Asphaltene Adsorption from Toluene on Dry Silica

Figure 7 gives the fifth overtone frequency ($\Delta f_5/5$, black) and dissipation (ΔD_5, red) kinetics relative to pure toluene for asphaltene adsorption and desorption from toluene on a dry silica surface. Each increase in asphaltene concentration leads to an additional step decline in frequency. Dissipation only slightly increases, consonant with a rigid or elastic adlayer. These two markers signify asphaltene adsorption according to the Sauerbrey term of eq 9 (or 10). Density–viscosity correction for the asphaltene–toluene solution is negligible. Zero dissipation change is consistent with negligible viscosity–density change and with a rigid adsorbed layer. The higher the asphaltene concentration, the larger is the adsorption amount ascertained from the Sauerbrey term in eq 10 relative to the toluene baseline.

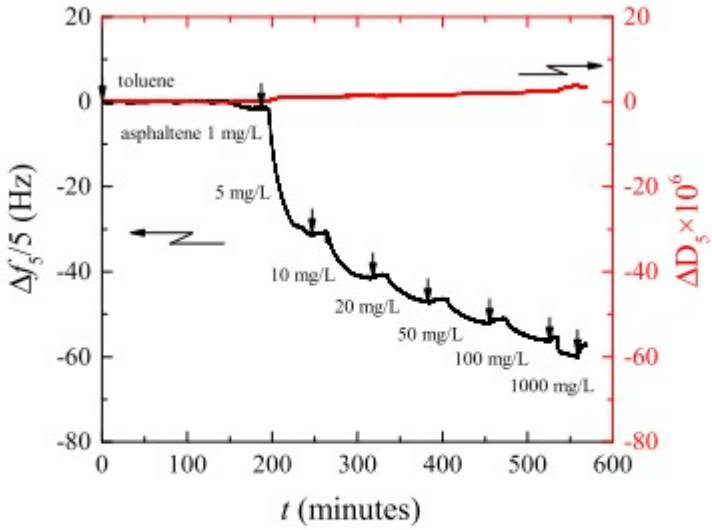

Figure 7. Sequence of frequency (black) and dissipation (red) kinetics (fifth overtone) for asphaltene adsorption from toluene on dry silica. Each injection step corresponds to increasing asphaltene concentration. Vertical arrows indicate injection of pure toluene before the subsequent higher asphaltene concentration.

Figure 8 shows the graph of asphaltene adsorption, $\hat{\Gamma}$ (mg/m^2), as a function of concentration in toluene after 30 min of exposure time. Black squares represent the experimental data. The solid line is calculated from the Langmuir expression(26)

$$\hat{\Gamma} = \frac{\hat{\Gamma}_{max} K c}{1 + K c} \quad (11)$$

where c is the asphaltene concentration (mg/L), $\hat{\Gamma}_{max}$ is the maximum adsorption (9.7 mg/m^2), and K is the Langmuir equilibrium constant (0.17 L/mg). Our measured amounts are in general agreement with the literature despite differences in asphaltene sources.(27−32) Asphaltene strongly adsorbs from toluene onto silica when not in the presence of water.

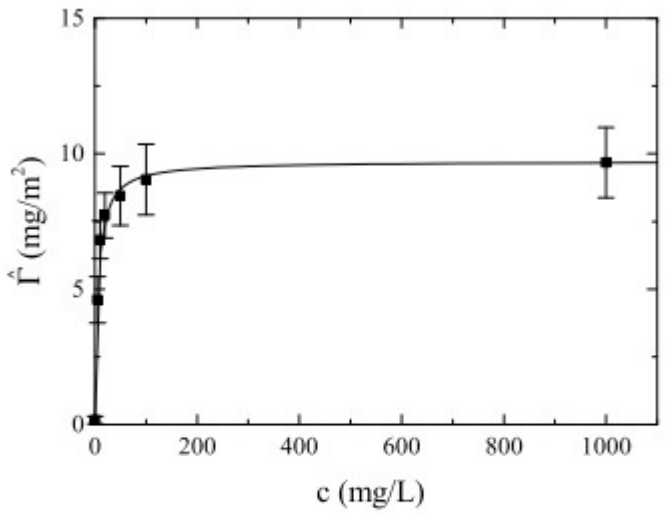

Figure 8. Asphaltene adsorption from toluene onto dry silica after 30 min exposure as a function of concentration (filled squares). The solid line corresponds to the Langmuir equation with $\hat{\Gamma}_{max}$ = 9.7 mg/m^2 and K = 0.17 L/mg. Typical error bar corresponds to measurement repeatability.

Following each increase in asphaltene concentration in Figure 7, but before the next increase, pure toluene is injected to desorb asphaltene (denoted by vertical arrows). There is only a small frequency increase after each ~25 min toluene flush. Most all the adsorbed asphaltene on dry silica is irreversibly bound. Thus, asphaltene adsorption from toluene onto dry silica is both strong and mostly irreversible. This conclusion is consistent with the available literature.(27−33) Agreement with the Langmuir equilibrium model in Figure 8 is inconsistent because of the observed irreversible attachment of toluene-solubilized asphaltene to the silica surface. However, slow rearrangement kinetics of initially reversible adsorbed configurations can lead to an early-time apparent Langmuir isotherm.(34,35)

Asphaltene Adsorption from Toluene through an Intervening Water Layer

Figure 9 shows an example of frequency dissipation kinetics for the injection sequence: water baseline, water-film deposition, pure toluene, loading of 15 mg/L asphaltene in toluene, and final toluene flush. The rise of frequency and fall in dissipation upon withdrawal of liquid water from the QCMD cell at 10 min correspond to the formation of a thin water layer in air. At 30 min, pure toluene is injected. Frequency declines and dissipation increases corresponding to replacing inviscid air in the cell by viscous toluene. Flushing of toluene for 50 min causes little change in signals, indicating that the water-layer thickness remains unchanged. At 80 min, a 15 mg/L asphaltene–toluene solution is injected with frequency falling and dissipation unchanging. We attribute this result to uptake of asphaltene from toluene onto the silica surface in the presence of the thin water layer. Finally, at 120

min, pure toluene is flushed with both frequency and dissipation remaining constant. We interpret this result as irreversible asphaltene adsorption.

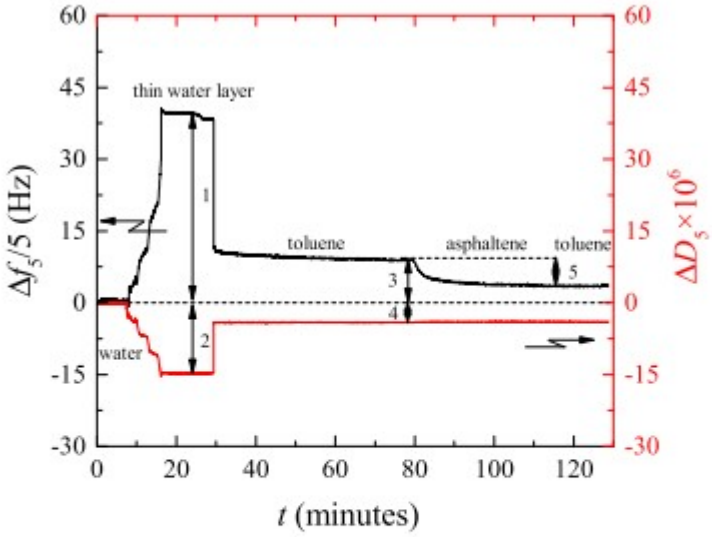

Figure 9. Frequency (black) and dissipation (red) kinetics (fifth overtone) for asphaltene adsorption from water-saturated toluene onto silica through a thin water layer. Injection sequence is: water baseline, water withdrawal, toluene, asphaltene in toluene (15 mg/L), and toluene flush. Thicknesses are from theory applied to the labeled frequency and dissipation differences: (1) $h_L \approx 47$ nm; (2) $h_L \approx 113$ nm; (3) $h_L \approx 37$ nm; (4) $h_L \approx 99$ nm; and (5) $\hat{\Gamma} \approx 1.5$ mg/m^2.

With $A = 1$, eq 3 (minus baseline correction from eq 5) and eq 4 (minus baseline correction from eq 6) specify water-film thicknesses in Figure 9 of 47 nm from frequency (labeled 1) and 113 nm from dissipation (labeled 2), respectively. Upon toluene injection at 30 min, theory in eq 3 evaluated with A from eq 2 (minus baseline correction from eq 5) gives a thickness from frequency of 37 nm (labeled 3) while eq 4 evaluated with A from eq 2 (minus baseline correction from eq 6) gives a water-film thickness of 99 nm (labeled 4). The frequency decline after injection of the 15 mg/L asphaltene solution is interpreted as asphaltene uptake (labeled 5) and quantified by the Sauerbrey expression as $\hat{\Gamma} = 1.5$ mg/m^2. Subsequent toluene flushing maintains this surface density.

We expect no change in water-layer thickness upon asphaltene adsorption. The experiment in Figure 9 was repeated for several different deposited water-layer thicknesses. Results are shown as filled squares in Figure 10, along with results (filled circles) from Gonzales and Taylor(16) for water films deposited onto silica by molecular vapor adsorption from humidified air. Our measurements from liquid water-film deposition concur with those reported by Gonzales and Taylor:(16) thicker water layers reduce asphaltene uptake. Even though specific asphaltene samples are different, uptake amounts are similar. However, we find that sorption reduction apparently requires thicker films than does reported by Gonzales and Taylor.(16) Water films larger than

~500 nm completely protect against asphaltene deposition. A thick water layer physically separates insoluble asphaltene molecules from the silica/water surface. In all cases, we find that when asphaltene attachment through water layers occurs, it is essentially irreversible.

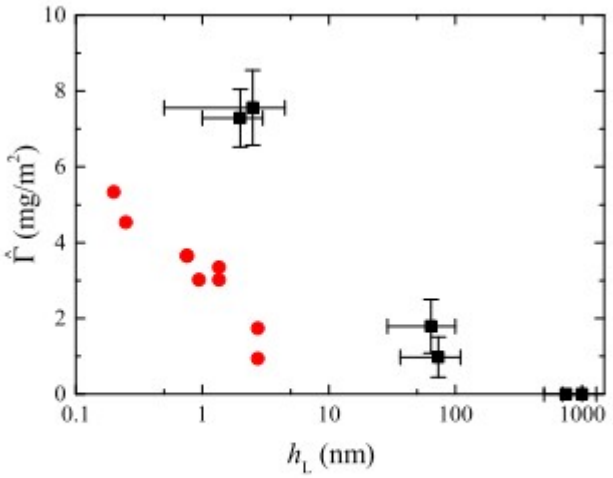

Figure 10. Influence of water thickness h_L on asphaltene adsorption from the toluene amount (filled squares). Filled circles are from Gonzalez and Taylor.[16] Asphaltene concentration is 15 mg/L.

Asphaltene molecules solubilized in oil do not dissolve into a surrounding water phase and adsorb onto a water-enveloped mineral surface. Rather asphaltene moieties at the oil/water interface molecularly deposit onto the solid surface when the protective water film breaks.(9,14,15) Our results in Figure 10 confirm that water layers defend against asphaltene deposition. Although the trend in Figure 10 of decreasing asphaltene sorption with increasing water-film thickness is consistent with that reported by Gonzales and Taylor,(16) the striking difference is that we record substantially thicker films. The films of Gonzales and Taylor(16) are molecular up to a few nm thickness. However, we detect much thicker films necessary to reduce asphaltene uptake. Direct contact of asphaltene-aggregate side-chain moieties dangling from an oil/water interface to a mineral surface demands molecularly thin intervening water films. An explanation for our contrary observation in Figure 10 emanates from Figure 1b. Thin water films sandwiched between an asphaltene–laden oil phase and a wetting solid surface are not likely homogeneous even for flat solid surfaces. Film rupture leaves behind trapped water microdroplets that average in a QCMD experiment to a thicker film than that ruptured between the microdroplets. (9) Asphaltene surface-attachment amounts in Figure 10 thus correspond to an average of drop-covered regions and regions between the microdrops where water layers are molecularly thin. We suggest that our thicker water films correspond to more water patches left behind. Consequently, the 500 nm water-film thickness for complete protection against asphaltene deposition in Figure 10 reflects a stable water film. Beyond this thickness,

wetting water films remain intact to protect against asphaltene attachment. Smaller thicknesses, however, break up allowing molecular asphaltene contact with the silica surface between microdrops.(9) We suggest that the discrepancies found in Figure 9 between film thicknesses calculated from frequency and from dissipation also arise from inhomogeneous water films.

The observations of Gonzales and Taylor(16) likely provide a more realistic estimate of water-layer thicknesses that prevent direct contact of oil/brine interface asphaltene moieties to a solid surface (i.e., around a few Angstroms). However, in reservoir application, water films deposit through a water-drainage process, not through molecular vapor adsorption. Inhomogeneous, ruptured water films are expected during drainage. Thus, thicker water films than those obtained by Gonzales and Taylor(16) are required to prevent asphaltene attachment to sandstone reservoir surfaces. Although our study focuses on pure water films, aqueous brine films are expected to behave similarly.

Conclusions

Asphaltene molecules and aggregates dissolved in crude oil play an overarching role in the behavior of oil reservoirs. Once attached to rock surfaces, asphaltene aggregates can produce local oil-wet regions that redistribute oil and water phases in the pore spaces. In this work, we form liquid–water films between silica and asphaltene–laden toluene by a drainage process in a QCMD flow cell. Continuum theory assesses the film thicknesses and the surface densities of attached asphaltene. We confirm the hypothesis that thick water films prevent attachment of asphaltene to a water-wet silica-mineral surface. In a drainage process, rupture of water films is prerequisite for the adhesion of asphaltene to a mineral surface. When protective water films rupture, attachment of asphaltene moieties to silica is irreversible. Water thicknesses required to prevent asphaltene deposition correspond to film stability. Once water films rupture, molecularly thin water layers apparently emerge that allow direct molecular contact of asphaltene to a mineral surface.

Acknowledgments

X.H. gratefully acknowledges the China Scholarship Council (CSC) and the National Natural Science Foundation of China (no. 51476130) for financial assistance during his stay at the University of California, Berkeley. S.H. was supported by the Ali I. Al-Naimi Petroleum Research Center (ANPERC) at the King Abdullah University of Science and Technology (KAUST), Thuwal, KSA.

References

(1) Morrow, N. R. Wettability and Its Effect on Oil Recovery. J. Pet. Technol. 1990, 42, 1476−1484. (2) Kovscek, A. R.; Wong, H.; Radke, C. J. A pore-level scenario for the development of mixed wettability in oil reservoirs. AIChE J. 1993, 39, 1072−1085. (3) Salathiel, R. A. Oil Recovery by Surface Film Drainage In MixedWettability Rocks. J. Pet. Technol. 1973, 25, 1216−1224.

(4) Sjöblom, J.; Simon, S.; Xu, Z. Model molecules mimicking asphaltenes. Adv. Colloid Interface Sci. 2015, 218, 1−16. (5) Adams, J. J. Asphaltene Adsorption, a Literature Review. Energy Fuels 2014, 28, 2831−2856. (6) Mullins, O. C.; Sabbah, H.; Eyssautier, J.; Pomerantz, A. E.; Barre, L.; Andrews, A. B.; Ruiz-Morales, Y.; Mostowfi, F.; McFarlane,´ R.; Goual, L.; Lepkowicz, R.; Cooper, T.; Orbulescu, J.; Leblanc, R. M.; Edwards, J.; Zare, R. N. Advances in Asphaltene Science and the Yen-Mullins Model. Energy Fuels 2012, 26, 3986−4003. (7) Langevin, D.; Argillier, J.-F. Interfacial behavior of asphaltenes. Adv. Colloid Interface Sci. 2016, 233, 83−93. (8) Buckley, J. S.; Takamura, K.; Morrow, N. R. Influence of Electrical Surface Charges on the Wetting Properties of Crude Oils. SPE Reservoir Eng. 1989, 4, 332−340. (9) Freer, E. M.; Svitova, T.; Radke, C. J. The role of interfacial rheology in reservoir mixed wettability. J. Pet. Sci. Eng. 2003, 39, 137− 158. (10) Jeribi, M.; Almir-Assad, B.; Langevin, D.; Henaut, I.; Argillier, J.´ F. Adsorption Kinetics of Asphaltenes at Liquid Interfaces. J. Colloid Interface Sci. 2002, 256, 268−272. (11) Cagna, A.; Esposito, G.; Quinquis, A.-S.; Langevin, D. On the reversibility of asphaltene adsorption at oil-water interfaces. Colloids Surf., A 2018, 548, 46−53. (12) Brady, P. V.; Morrow, N. R.; Fogden, A.; Deniz, V.; Loahardjo, N.; Winoto. Electrostatics and the Low Salinity Effect in Sandstone Reservoirs. Energy Fuels 2015, 29, 666−677. (13) Schmatz, J.; Urai, J. L.; Berg, S.; Ott, H. Nanoscale imaging of pore-scale fluid-fluid-solid contacts in sandstone. Geophys. Res. Lett. 2015, 42, 2189−2195. (14) Buckley, J. S.; Morrow, N. R. Characterization of Crude Oil Wetting Behavior by Adhesion Tests. SPE/DOE Enhanced Oil Recovery Symposium: Tulsa, Oklahoma, 1990. (15) Buckley, J. S. Evaluation of Reservoir Wettability and its Effect on Oil Recovery. US DOE Report, 1999, DE-FC22-96ID13421. (16) Gonzalez, V.; Taylor, S. E. Asphaltene adsorption on quartz sand in the presence of pre-adsorbed water. J. Colloid Interface Sci. 2016, 480, 137−145. (17) Asay, D. B.; Kim, S. H. Evolution of the Adsorbed Water Layer Structure on Silicon Oxide at Room Temperature. J. Phys. Chem. B 2005, 109, 16760−16763. (18) Johannsmann, D. The Quartz Crystal Microbalance in Soft Matter Research: Fundamentals and Modeling; Springer: New York, 2015. (19) Reviakine, I.; Johannsmann, D.; Richter, R. P. Hearing What You Cannot See and Visualizing What You Hear: Interpreting Quartz Crystal Microbalance Data from Solvated Interfaces. Anal. Chem. 2011, 83, 8838−8848. (20) Spiecker, P. M.; Gawrys, K. L.; Kilpatrick, P. K. Aggregation and solubility behavior of asphaltenes and their subfractions. J. Colloid Interface Sci. 2003, 267, 178−193. (21) Wang, L.; Siretanu, I.; Duits, M. H. G.; Stuart, M. A. C.; Mugele, F. Ion effects in the adsorption of carboxylate on oxide surfaces, studied with quartz crystal microbalance. Colloids Surf., A 2016, 494, 30−38. (22) Voinova, M. V.; Rodahl, M.; Jonson, M.; Kasemo, B. Viscoelastic acoustic response of layered polymer films at fluid-solid interfaces: Continuum mechanics approach. Phys. Scr. 1999, 59, 391− 396. (23) Sauerbrey, G. Verwendung von Schwingquarzen zur Wagung¨ dünner Schichten und zur Mikrowagung.¨ Z. Phys. 1959, 155, 206− 222. (24) Bretherton, F. P. The motion of long bubbles in tubes. J. Fluid Mech. 1961, 10, 166−188. (25)

Erzuah, S.; Fjelde, I.; Voke Omekeh, A. Wettability Estimation by Oil Adsorption Using Quartz Crystal Microbalance with Dissipation QCM-D. SPE Europec featured at 80th EAGE Conference and Exhibition; Society of Petroleum Engineers: Copenhagen, Denmark, 2018. (26) Berg, J. C. An Introduction to Interfaces & Colloids: The Bridge to Nanoscience; World Scientific: Singapore, 2010. (27) Ekholm, P.; Blomberg, E.; Claesson, P.; Auflem, I. H.; Sjöblom, J.; Kornfeldt, A. A Quartz Crystal Microbalance Study of the Adsorption of Asphaltenes and Resins onto a Hydrophilic Surface. J. Colloid Interface Sci. 2002, 247, 342−350. (28) Dudaśovaˇ , D.; Silset, A.; Sjo´ ¨blom, J. Quartz Crystal Microbalance Monitoring of Asphaltene Adsorption/Deposition. J. Dispersion Sci. Technol. 2008, 29, 139−146. (29) Farooq, U.; Sjöblom, J.; Øye, G. Desorption of Asphaltenes from Silica-Coated Quartz Crystal Surfaces in Low Saline Aqueous Solutions. J. Dispersion Sci. Technol. 2011, 32, 1388−1395. (30) Kelesoǵˇlu, S.; Volden, S.; Kes, M.; Sjöblom, J. Adsorption of Naphthenic Acids onto Mineral Surfaces Studied by Quartz Crystal Microbalance with Dissipation Monitoring (QCM-D). Energy Fuels 2012, 26, 5060−5068. (31) Abudu, A.; Goual, L. Adsorption of Crude Oil on Surfaces Using Quartz Crystal Microbalance with Dissipation (QCM-D) under Flow Conditions. Energy Fuels 2009, 23, 1237−1248. (32) Hannisdal, A.; Ese, M.-H.; Hemmingsen, P. V.; Sjöblom, J. Particle-stabilized emulsions: Effect of heavy crude oil components pre-adsorbed onto stabilizing solids. Colloids Surf., A 2006, 276, 45− 58. (33) Yang, G.; Chen, T.; Zhao, J.; Yu, D.; Liu, F.; Wang, D.; Fan, M.; Chen, W.; Zhang, J.; Yang, H.; Wang, J. Desorption Mechanism of Asphaltenes in the Presence of Electrolyte and the Extended Derjaguin-Landau-Verwey-Overbeek Theory. Energy Fuels 2015, 29, 4272−4280. (34) Maurer, S. A.; Bedbrook, C. N.; Radke, C. J. Competitive Sorption Kinetics of Inhibited Endo- and Exoglucanases on a Model Cellulose Substrate. Langmuir 2012, 28, 14598−14608. (35) Cascao Pereira, L. G.; Hickel, A.; Radke, C. J.; Blanch, H. W. A˜ kinetic model for enzyme interfacial activity and stability: pahydroxynitrile lyase at the diisopropyl ether/water interface. Biotechnol. Bioeng. 2002, 78, 595−605.